Received: 1 October 2021 | Revised: 31 March 2022 | Accepted: 4 May 2022

DOI: 10.1111/jeb.14025

JOURNAL OF Evolutionary Biology eseb

RESEARCH ARTICLE

Correlated evolution between orb weaver glue droplets and supporting fibres maintains their distinct biomechanical roles in adhesion

Sean D. Kelly[1,2] | Brent D. Opell[3] | Sandra M. Correa-Garwhal[4]

[1]Department of Biology, San Diego State University, San Diego, California, USA

[2]Evolution, Ecology, and Organismal Biology Department, University of California Riverside, Riverside, California, USA

[3]Department of Biological Sciences, Virginia Tech, Blacksburg, Virginia, USA

[4]American Museum of Natural History, New York, New York, USA

Correspondence
Sean D. Kelly, Joint Doctoral Program in Evolutionary Biology
San Diego State University and University of California Riverside
San Diego, CA, USA.
Email: skelly0576@sdsu.edu

Funding information
National Science Foundation, Grant/Award Number: IOS-1755028

Abstract

Orb weaving spiders employ a 'silken toolkit' to accomplish a range of tasks, including retaining prey that strike their webs. This is accomplished by a viscous capture spiral thread that features tiny glue droplets, supported by a pair of elastic flagelliform fibres. Each droplet contains a glycoprotein core responsible for adhesion. However, prey retention relies on the integrated performance of multiple glue droplets and their supporting fibres, with previous studies demonstrating that a suspension bridge forms, whose biomechanics sum the adhesive forces of multiple droplets while dissipating the energy of the struggling insect. While the interdependence of the droplet's glycoprotein and flagelliform fibres for functional adhesion is acknowledged, there has been no direct test of this hypothesized linkage between the material properties of each component. Spider mass, which differs greatly across orb weaving species, also has the potential to affect flagelliform fibre and glycoprotein material properties. Previous studies have linked spider mass to capture thread performance but have not examined the relationship between spider mass and thread material properties. We extend earlier studies to examine these relationships in 16 orb weaving species using phylogenetic generalized least squares. This analysis revealed that glycoprotein stiffness (elastic modulus) was correlated with flagelliform fibre stiffness, and that spider mass was related to the glycoprotein volume, flagelliform fibre cross-sectional area and droplets per unit thread length. By shaping the elastic moduli of glycoprotein adhesive and flagelliform fibres, natural selection has maintained the biomechanical integration of this adhesive system.

KEYWORDS
bioadhesive, biomechanics, capture thread, flagelliform fibres, glycoprotein, orb weaver

1 | INTRODUCTION

Natural adhesives can facilitate locomotion or permanently attach animals. Arboreal leaf-cutter ants that carry heavy loads as they climb in the forest canopy rely on adhesive tarsi and the tube feet of sea urchins allow these animals to resist strong underwater currents as they move (Santos et al., 2009; Stark et al., 2019). In contrast, the bioadhesives that attach barnacles and mussels to wet and salt-encrusted surfaces harden rapidly and permanently (Dickinson et al., 2009; Waite, 2017). Other organisms use viscous adhesives

that remain pliable to capture prey. Sundews use sticky droplets on their leaves for this purpose (Huang et al., 2015; Olivencia et al., 1995) and araneoid orb weaving spiders use capture threads comprised of tiny glue droplets supported by extensible flagelliform fibres to retain insects that strike a web (Figure 1) (Opell, Clouse, & Andrews, 2018; Sahni et al., 2010). In each case these adhesives are widely distributed, allowing them to 'sit and wait' for prey (Blackledge et al., 2011; Uetz et al., 1978).

An orb web supports the elastic capture thread with stiffer major ampullate silk that radiates from the centre of the web and in many species is responsible for absorbing the kinetic energy of prey impact (Blackledge & Hayashi, 2006; Sensenig et al., 2010, 2012; Swanson et al., 2006). The capture thread, which is suspended between these radii, is produced by spigots on the median spinnerets (Coddington, 1989). As a flagelliform fibre emerges from a spigot on each spinneret it is coated with an aqueous solution of proteins, containing low molecular mass compounds (LMMCs), and inorganic salts, issuing from two flanking aggregate gland spigots (Opell, Jain, et al., 2018). When the coated fibres from each spinneret unite, this composite cylinder quickly self-organizes into regularly spaced droplets, due to Plateau - Rayleigh instability (Figure 1a,b) (Edmonds & Vollrath, 1992; Mead-Hunter et al., 2012). A glycoprotein core condenses within each droplet leaving the remaining material and amorphous proteins in an aqueous layer that covers both the flagelliform fibres within and between droplets (Amarpuri, Chaurasia, et al., 2015; Vollrath & Tillinghast, 1991). The even spacing of these droplets ensures that the adhesive is deployed in a parsimonious manner (Blackledge & Gillespie, 2002). A cylindrical centre of the core (termed a granule) appears to be responsible for anchoring the glycoprotein to the flagelliform fibre, although it is possible to slide droplets along a flagelliform fibre and this can occur naturally as a thread's suspension bridge begins to fail (Opell & Hendricks, 2010; Sahni et al., 2010; Tillinghast et al., 1993; Kelly, unpublished observations).

The adhesive performance of the glycoprotein core is conditioned by the LMMCs in the surrounding aqueous layer, whose composition differs among species (Amarpuri, Zhang, et al., 2015; Jain et al., 2018; Opell, Jain, et al., 2018). These compounds solvate the adhesive glycoprotein, softening it and improving its adhesion (Sahni et al., 2014; Singla et al., 2018). The LMMCs also confer hygroscopicity to the droplets, allowing droplet volume to respond to changes in atmospheric humidity (Edmonds & Vollrath, 1992; Opell, Jain, et al., 2018; Townley et al., 1991; Townley & Tillinghast, 2013). However, LMMC concentration alone may not determine droplet hygroscopicity, as these compounds interact with a droplet's proteins (Jain et al., 2018).

Much like the closely packed glue stalks of sundews, the capture thread droplets of orb webs work together to increase adhesion (Krausko et al., 2017). Moreover, successful adhesion is often the result of multiple threads contacting an insect, which may manifest itself in a suspension bridge configuration (Figure 1) (Chacón & Eberhard, 1980). The biomechanics of this configuration sum the adhesive forces of multiple droplets along the thread, generating greater adhesion with greater thread length, although there may be diminishing returns at a certain length (Opell & Hendricks, 2009). As it forms, this suspension bridge also absorbs some of the force of a prey's struggles to escape by simultaneously incorporating the work done in stretching both the droplets and the flagelliform fibres (Opell et al., 2008; Sahni et al., 2010, 2011). The elastic (Young's) modulus or stiffness of each capture thread component and the amount of each material determines their contributions to this crucial phase of prey capture (Opell et al., 2019; Sahni et al., 2010). Initial modelling of the suspension bridge adhesive delivery system predicted that exterior (and more extended) droplets contribute more adhesion than interior droplets (Figure 1c) (Opell & Hendricks, 2009). However, recent work has cast doubt on the universal nature of this model (Opell & Stellwagen, 2019). While this aspect of the system may be variable, modelling reveals that suspension bridges are robust, with a random distribution of droplets not deteriorating adhesive load bearing or energy absorption (Guo et al., 2019).

An effective suspension bridge relies on contributions from both capture thread components as well as their integration within the system. Indeed, evidence shows that the suspension bridge relies on a linkage between the flagelliform fibres and adhesive glycoprotein,

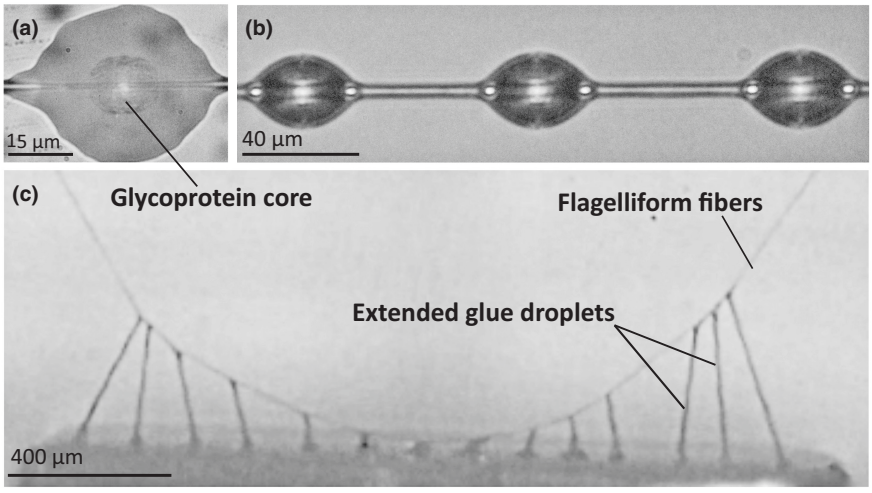

FIGURE 1 Araneoid capture thread: (a) flattened droplet of *Argiope aurantia* revealing its glycoprotein core. (b) a view of the capture spiral thread, showing the evenly spaced ellipsoid droplets of *Neoscona crucifera*. (c). The suspension bridge configuration of *Verrucosa arenata*, with bowing flagelliform fibres and extending glycoprotein droplets

with changes in the material properties of either component reducing thread adhesion (Guo et al., 2018). The codependence of the capture thread constituents predicts that, as orb weavers have diversified and adapted to different habitats, the material properties of both have evolved in a synergistic manner to maintain the functionality of the bridge. This 'synergy hypothesis' predicts that changes in the material properties of one capture thread component will be associated with scaled changes in the other. Here, we test this hypothesis by comparing the elastic modulus and toughness of each thread component. Additionally, we compare the material investment in a thread's adhesive glycoprotein and flagelliform fibres.

The stiffness of flagelliform fibres differs greatly among orb weaving species (Sensenig et al., 2010). Therefore, we predict that more extensible glue droplets will be associated with more extensible flagelliform fibres. We also predict that the toughness and the material investment in these two thread components will exhibit a similar association. Literature suggests that larger spiders spin larger webs and threads with larger glue droplets (Sensenig et al., 2010). Mature females of the 16 species that we studied exhibited a 117-fold difference in mass (Table 1). Therefore, we also examined the relationship of spider mass on capture silk material properties and on the amounts of material invested in each capture thread component. We use phylogenetic generalized least squares (PGLS) to examine these associations among orb weavers.

2 | MATERIALS AND METHODS

2.1 | Study species

We selected 14 species of spiders found near Blacksburg, Virginia for study for which 10–14 webs of mature females could be obtained (Figure 2). In doing this, we were able to represent the phylogenetic, size and habitat diversity of araneoid orb weavers reasonably well. We added one species each from south-eastern Arizona and southern California, which built webs in large laboratory enclosures to include three species each in the genera *Argiope* and *Neoscona* for a total of 16 species (Figure 2). These two species, *Argiope argentata* and *Neoscona oaxacensis* were the only species where the spiders themselves were collected. Covering two families, our selected orb-web weavers contain four groups of congeneric species, allowing us to contrast thread properties within genera. Adult females of these species differ greatly in mean mass, with *Cyclosa turbinata* weighing 7.2 mg compared to *Argiope aurantia* at 841.9 mg (Opell & Hendricks, 2009). The capture spiral configuration among these species differs as well, with droplets per mm thread length exhibiting a 10-fold difference and droplet volume a 40-fold difference (Table 1). These orb-web weavers forage in various habitats, with some occupying open weedy areas and others occupying forest interiors (Bradley, 2013).

TABLE 1 General spider and thread features

Species	Spider mass (mg)	Droplets per mm	Droplet volume $\mu m^3 \times 10^3$	Glycoprotein volume $\mu m^3 \times 10^3$	Flagelliform CSA μm^2
Araneus marmoreus	498.5 ± 74.2[c]	4.4 ± 0.8	105.7 ± 15.0[a]	39.4 ± 14.3[a]	**22.7 ± 2.7**[b]
Araneus pegnia	65.7 ± 7.1[c]	13.9 ± 3.1	7.1 ± 1.6[a]	5.0 ± 1.2[a]	10.4 ± 0.2[a]
Argiope argentata	337.6 ± 32.6	14.76 ± 0.57	14.1 ± 1.6	3.1 ± 0.6	12.1 ± 1.1
Argiope aurantia	841.9 ± 138.7[c]	3.3 ± 0.3	86.1 ± 16.5[a]	10.7 ± 2.4[a]	**36.2 ± 3.5**[b]
Argiope trifasciata	510.8 ± 82.0[c]	9.8 ± 1.3	41.6 ± 6.9[a]	31.5 ± 5.6[a]	**13.2 ± 1.3**[b]
Cyclosa turbinata	7.2 ± 0.8[c]	33.4 ± 6.9	2.2 ± 0.6	0.9 ± 0.2	**1.3 ± 0.02**[b]
Larinioides cornutus	265.9 ± 27.2[c]	13.1 ± 1.8	4.8 ± 0.7[a]	1.8 ± 0.4[a]	**10.6 ± 0.9**[b]
Leucauge venusta	22.0 ± 3.1[c]	21.4 ± 2.5	1.4 ± 0.2[a]	0.6 ± 0.1[a]	**1.3 ± 0.1**[b]
Metepeira labyrinthea	**46 ± 14**[b]	10.6 ± 2.7	3.4 ± 0.7[a]	1.4 ± 0.3[a]	**3.5 ± 0.3**[b]
Micrathena gracilis	73.4 ± 9.5[c]	6.2 ± 1.5	7.5 ± 1.5[c]	1.9 ± 0.3[a]	**2.7 ± 0.1**[b]
Micrathena sagittata	46.8 ± 5.5[c]	5.5 ± 1.2	8.7 ± 0.8[a]	2.6 ± 0.2[a]	6.7 ± 0.2[a]
Neoscona arabesca	**46 ± 24**[b]	9.0 ± 1.0	2.5 ± 0.6	1.0 ± 0.3	**4.5 ± 0.4**[b]
Neoscona crucifera	**368 ± 142**[b]	8.7 ± 1.0	13.4 ± 1.7[a]	2.6 ± 0.7[a]	**14.1 ± 2.2**[b]
Neoscona oaxacensis	166.85	10.65 ± 1.06	5.9 ± 0.7	0.6 ± 0.1	7.6 ± 1.9
Tetragnatha elongata	71.0 ± 17.2[c]	14.8 ± 2.2	2.7 ± 0.7[a]	1.1 ± 0.3[a]	3.2 ± 0.3
Verrucosa arenata	74.3 ± 12.2[c]	7.3 ± 0.5	10.3 ± 1.7[a]	1.8 ± 0.4[a]	**3.5 ± 0.6**[b]

Measurements were taken at 50%–55% relative humidity. *N. Oaxcensis* mass is from Greenstone & Bennet, 1980. Sample size differs, given the range of sources. We determined droplets per millimetre by placing our 2 mm scale along a capture thread and divided the counted droplets by two. Means ± SD in bold and ± S.E. elsewhere.

Abbreviation: CSA, Cross-sectional area.

[a]Indicates Opell et al., 2021.

[b]Indicates Sensenig et al., 2010.

[c]Indicates Opell & Hendricks, 2009.

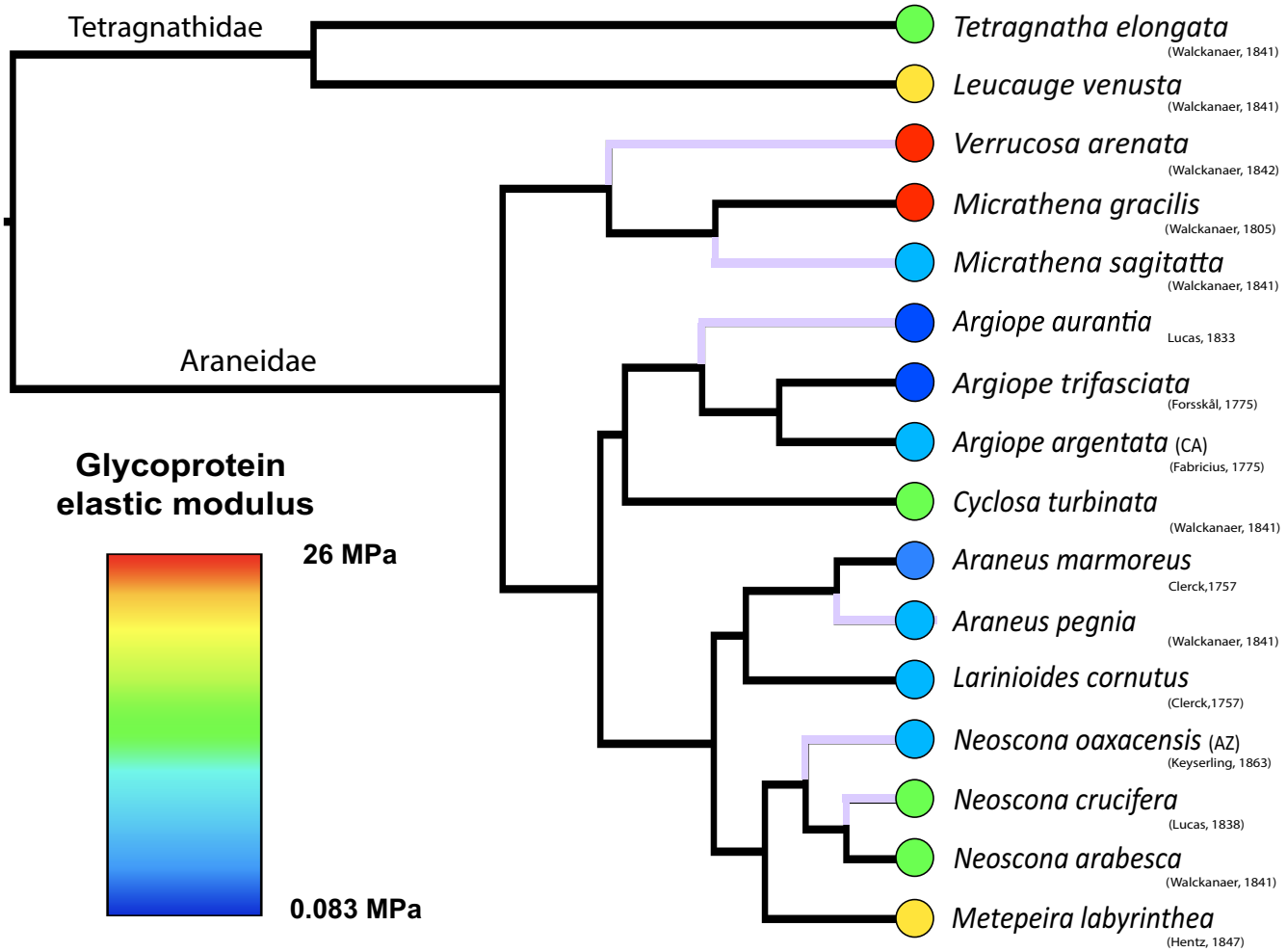

FIGURE 2 Phylogeny of study species and their elastic moduli: Topology is primarily based on a phylogenetic tree from Dimitrov et al., 2017, with modifications to add *Argiope argentata* and *Verrucosa arenata* (based on Garrison et al., 2016, Scharff et al., 2019, respectively). Subsequent taxa were added based on their congener's presence within the tree. Species added to our input tree have coloured branches

2.2 | Web collection

We collected orb-web samples shortly after they were constructed, ensuring fresh threads that were uncontaminated by dust or pollen. A metal frame with double sided tape (3 M #9086K29550360) on its rim was pressed from behind a web, ensuring that a web's native tensions were preserved. Once adhered to the taped rim, the remaining web was separated by hand along the outer edge of the frame, isolating the sample. After collecting a web, each site was marked with flagging tape to prevent resampling. Spiders were unharmed by this process, fleeing their webs as samples were taken and were usually found with a new web in the same location the following day. The masses of all species except *Argiope argentata*, which was determined for individuals whose threads we studied, were taken from the literature (Greenstone & Bennett, 1980; Opell & Hendricks, 2009; Sensenig et al., 2010). An advantage of this work is its non-destructive nature, with our collecting posing no more of a threat to a spider than a rainy day. Once collected, webs were placed in a box to prevent contamination from pollen or further damage, returned to the laboratory, and all testing completed by 16:00 on the day of collecting, except for the nocturnal species *Larinioides cornutus* and *Neoscona crucifera*, whose web samples were collected in the evening of the previous day.

2.3 | Thread preparation and individual droplet testing

To prepare individual droplets for testing, we collected a thread on carbon tape covered forceps to ensure natural thread tension was maintained (Cat #77816, Electron Microscope Sciences, Hatfield, PA, USA). These forceps are blocked open to accommodate the width of supports on a microscope slide sampler. After contacting a thread strand with the forceps, we cut the connecting threads with a pair of iris scissors. This sample then spanned the 4.8 mm space between the supports of a microscope slide sampler (Opell et al., 2011). We ensured that these threads were perpendicular to the supports, guaranteeing consistency in the length of the tested thread and the angle of droplet extension.

To ensure that only a single droplet contacted our probe, we isolated the central droplet of the suspended strand. Droplets on either side were slid away from the central droplet using a wooden applicator stick that was whittled to a fine tip, exposing a few xylem fibres. When wetted with distilled water, droplets could easily be moved along the supporting strand. This did not disrupt the aqueous layer of the flagelliform fibres, documented by the formation of small secondary droplets near the central droplet. Once prepared, this slide was placed into a sealed, glass-covered chamber on the mechanical stage of a Mitutoyo FS60 inspection microscope (Mitutoyo America Corp., Aurora, IL, USA). Chamber temperature was maintained at 23°C by a thermostat-controlled Peltier thermocouple. The probe of a Fisher Scientific® Instant Digital Hygrometer, which extended through the chamber allowed us to monitor humidity and establish 55% relative humidity (RH) testing conditions. A small piece of distilled water moistened Kimwipe® in the chamber increased humidity above ambient laboratory humidity and rising humidity was offset by drawing a small amount of room air into the chamber through a tube attached to a port in the chamber wall. These conditions were comparable to those of other investigators' laboratories where the material properties of capture thread flagelliform fibres were determined (approximately 50% RH and 23 degrees C).

With the desired humidity achieved, droplets were extended using a probe. Before each test, the 413 μm tip of this polished steel probe was cleaned with 100% ethanol on a Kimwipe® or Whatman® filter paper. After inserting the probe into a port in the side of the chamber, the probe was locked into a support resting beside the microscope to prevent its movement (Opell, Clouse, & Andrews, 2018). The isolated droplet was then brought into contact with the probe tip using the microscope's mechanical stage. To ensure droplet adhesion, the stage was then advanced an additional 250 - 500 μm. The movement of the stage was then reversed by a stepping motor, extending the droplet at a velocity of 69.5 μms^{-1} until the droplet pulled free of the probe. During this time, a video was recorded with a Canon digital Rebel T2i at 60 frames per second. Close examination of these videos showed that nearly all droplets pulled cleanly from the probe, leaving no visible protein residue. This is consistent with findings that a short glue droplet contact period resulted in complete adhesive peeling and clean droplet release (Amarpuri et al., 2017; Kelly et al., 2019).

The volume of a droplet's glycoprotein core is required for computations of elastic modulus and glycoproteins are most easily visualized when droplets are flattened. To accomplish this, we placed additional thread samples into our glass-covered observation chamber. We photographed three droplets along the suspended thread before flattening the thread by dropping a glass coverslip onto it from a magnetically tripped device within the chamber. We photographed these droplets again within 30 s after they were flattened. To compute droplet volume, we first measured the length (DL, dimension parallel to the thread) and width (DW) of each suspended droplet using ImageJ 1.50i (https://imagej.nih.gov/ij/). Using these measurements, droplet volume (DV) was determined with the following formula (Liao et al., 2015).

$$DV = \frac{2\pi \times DW^2 \times DL}{15} \quad (1)$$

From images of each of an individual's three flattened droplets, we measured droplet surface area and glycoprotein surface area. Dividing droplet volume by droplet surface area yields the thickness of a flattened droplet's glycoprotein core. Obtaining droplet thickness allowed us to calculate glycoprotein volume by multiplying thickness by glycoprotein surface area. The mean of an individual's ratio of glycoprotein volume to droplet volume was then used to infer the glycoprotein volume within this individual's extended droplets.

2.4 | Adhesive glycoprotein material properties

The glycoprotein properties of 11 species (*A. aurantia*, *Araneus marmoreus*, *Argiope trifasciata*, *L. cornutus*, *Leucauge venusta*, *Metepeira labyrinthea*, *Micrathena gracilis*, *Micrathena sagittata*, *N. crucifera*, *Tetragnatha elongata* and *Verrucosa arenata*) were taken from the literature (Opell et al., 2021). The values of *Tetragnatha elongata*, which in this earlier study were based on the flagelliform fibre properties of *Tetragnatha versicolor*, have been updated to reflect newly determined *T. elongata* flagelliform fibre diameter and elastic modulus values (Table 2). We added glycoprotein properties of four additional species (*A. argentata*, *C. turbinata*, *N. arabesca* and *N. oaxacensis*).

Individual droplet extension videos allowed us to generate true stress–strain curves, from which we determined the glycoprotein core's elastic modulus. These are based on true stress and true strain values determined at the initiation of droplet extension and at each 20% extension time intervals though droplet pull-off. In some species from low humidity habitats, whose droplets are very hygroscopic, tiny aqueous droplets form along the extending droplet, exposing its protein filament to the drying effects of air. This condition is not characteristic of the droplets in a normal suspension bridge configuration and has been termed Phase 2 extension (Opell, Jain, et al., 2018). This contrasts to more typical Phase 1 extension during which a droplet's glycoprotein remains covered by aqueous material during extension and pull-off. When we encountered Phase 2 extensions, we restricted our characterization of glycoprotein to the portion of the extension during which glycoprotein was surrounded by aqueous material.

At each of the five reference points during droplet extension, we used the deflection angle of a droplet's support line to gauge force on the droplet's protein filament during extension. The computations described below rely on the diameters and elastic modulus of each species' flagelliform fibres whose determination is described in a subsequent paragraph. The seven steps used to construct these curves are described mathematically in Figure 3. Steps 1 and 2 compute the extension of the flagelliform fibres from the angular deflection of the 4800 μm long support line to determine the forces exerted on the extending droplet. Steps 3 and 4 resolve these force vectors and determine the force on the extending droplet. Steps 5 and 6 compute true stress on the droplet filament by dividing this force by the protein filament's cross-sectional area, determined as

TABLE 2 Capture silk material properties

Species	Glycoprotein volume per mm of thread $\mu m^3 \times 10^3$	Flagelliform volume per mm of thread $\mu m^3 \times 10^3$	Glycoprotein elastic modulus, MPa	Flagelliform elastic modulus, MPa	Glycoprotein toughness, MJ/m^3	Flagelliform toughness, MJ/m^3
Araneus marmoreus	173.3 ± 63.0[a]	**22.7 ± 2.7**[b]	0.26 ± 0.25[a]	**5 ± 2**[b]	0.51 ± 0.32[a]	**163 ± 64**[b]
Araneus pegnia	68.8 ± 16.2[a]	10.4 ± 0.2[a]	0.77 ± 0.22[a]	3.15 ± 0.7[a]	2.05 ± 0.96[a]	10.3 ± 2.6[a]
Argiope argentata	46.4 ± 1.8	12.1 ± 1.1	0.50 ± 0.21	1.81 ± 0.19	0.51 ± 0.20	50 ± 5
Argiope aurantia	35.5 ± 7.8[a]	**36.2 ± 3.5**[b]	0.08 ± 0.05[a]	**9 ± 11**[b]	0.22 ± 0.09[a]	**211 ± 99**[b]
Argiope trifasciata	308.8 ± 55.1[a]	**13.2 ± 1.3**[b]	0.09 ± 0.05[a]	**8 ± 5**[b]	0.63 ± 0.31[a]	**185 ± 65**[b]
*Cyclosa turbinata**	29.2 ± 7.7	**1.3 ± 0.02**[b]	1.32 ± 0.62	**22 ± 18**[b]	0.12 ± 0.04	**52 ± 28**[b]
Larinioides cornutus	24.1 ± 4.7[a]	**106.2 ± 0.9**[b]	0.48 ± 0.15[a]	**11 ± 8**[b]	0.55 ± 0.19[a]	**225 ± 84**[b]
Leucauge venusta	13.7 ± 2.2[a]	**1.3 ± 0.1**[b]	4.85 ± 1.26[a]	**58 ± 46**[b]	7.10 ± 1.17[a]	**148 ± 74**[b]
Metepeira labyrinthea	14.4 ± 3.5[a]	**3.5 ± 0.3**[b]	3.16 ± 0.85[a]	**13 ± 19**[b]	4.91 ± 1.55[a]	**123 ± 48**[b]
Micrathena gracilis	11.7 ± 1.6[a]	**2.7 ± 0.1**[b]	9.26 ± 2.49[a]	**52 ± 53**[b]	17.08 ± 2.49[a]	**53 ± 24**[b]
Micrathena sagittata	14.3 ± 1.3[a]	6.7 ± 0.2[a]	0.73 ± 0.25[a]	2.78 ± 0.6[a]	2.10 ± 0.43[a]	23.9 ± 6.9[a]
Neoscona arabesca	9.0 ± 2.4	**4.5 ± 0.4**[b]	1.06 ± 0.36	**22 ± 13**[b]	0.08 ± 0.03	**133 ± 73**[b]
Neoscona crucifera	22.4 ± 6.0[a]	**14.1 ± 2.2**[b]	1.74 ± 0.64[a]	**10 ± 5**[b]	1.49 ± 0.51[a]	**252 ± 99**[b]
Neoscona oaxacensis	6.7 ± 0.7	7.6 ± 1.9	0.66 ± 0.23	6.2 ± 0.8	1.25 ± 0.49	117 ± 17
Tetragnatha elongata	17.4 ± 4.1[a]	3.2 ± 0.3	1.25 ± 0.70	18 ± 2	0.47 ± 0.31	149 ± 11
Verrucosa arenata	13.0 ± 2.9[a]	**3.5 ± 0.6**[b]	26.08 ± 7.82[a]	**98 ± 19.9**[b]	28.19 ± 8.86[a]	**272 ± 80**[b]

Means ± SD in bold and S.E. elsewhere. These pairs were analysed using PGLS (phylogenetic generalized least squares) to compare the material properties of each capture silk component. 2010 Species with * are members of the same genus as their counterpart in Sensenig et al., 2010.

[a]Indicates data from Opell et al., 2021.

[b]Indicates Sensenig et al., 2010.

protein volume divided by droplet length). Step 7 determines true strain on a droplet at length DE using the diameter of the droplet's protein core when configured as a sphere as initial droplet length (Figure 3).

Each stress–strain curve from which a glycoprotein's elastic modulus and toughness were determined was constructed from measurements of droplet lengths and support line deflection angles taken at 20% intervals from 0% to 100% extension (0% being just prior to droplet extension and 100% being just before droplet pull-off). Elastic modulus was determined as the linear portion of each curve. Unlike typical stress–strain curves, which begin with a stress of zero, droplets are under tension prior to extension. Consequently, when glycoprotein toughness was computed, we subtract the thin rectangular area defined by the stress at the initial extension and maximum strain from the full area under the curve.

2.5 | Determining flagelliform fibre properties

Flagelliform fibre properties of *A. pegnia*, *A. argentata*, *M. sagittatta* and *N. oaxacensis*, and *T. elongata* capture threads were newly measured. Those of other species are taken from the literature (Sensenig et al., 2010). Flagelliform fibre diameter was measured from capture threads mounted in microscope immersion oil under a glass coverslip. Additional threads from each individual's web were secured to cardboard samplers and sent to the American Museum of Natural History for characterization of their elastic modulus and toughness using a Nano Bionix instrument (Agilent Technologies, Oak Ridge, TN, USA). Similar methodology and instrumentation was used by Sensenig et al., 2010 to determine these properties for eleven of the study species present in the literature. The flagelliform fibre features of *C. conica* were used for the similarly sized species *C. turbinata* included in this study (Sensenig et al., 2010).

2.6 | Evolutionary analyses and software

We used phylogenetic generalized least squares (PGLS) to examine relationships among the capture thread material properties under Brownian Motion, with Pagel's lambda to detect phylogenetic signal (Pagel, 1999). This method accounts for the evolutionary relatedness among species, ensuring that our analysis is not biased by these relationships (Felsenstein, 1985; Garamszegi, 2014). The phylogeny used in this analysis is based on a time calibrated tree produced from BEAST (Dimitrov et al., 2017). This phylogeny contains many of our focal species, but *Tetragnatha elongata* and *C. turbinata* were substituted for their congeners: *Tetragnatha versicolor* and *Cyclosa conica*. With these substitutions, we used the phytools R package to prune the tree to 10 species that were present in the phylogeny and our material property data set (R Core Team, 2019; Revell, 2012). The absence of our remaining six study species: *A. pegnia*, *A. aurantia*, *N. crucifera*, *N. oaxacensis*, *M. sagitatta* and *V. arenata* required further editing. Lacking data on the precise phylogenetic placement of these taxa, we placed them halfway along the length of their sister's branch when present (*A. pegnia*, *M. sagitatta*). *Verrucosa arenata* had no sister taxa in our phylogeny, so its placement was approximated using a different phylogenetic study, which placed it as an outgroup of the genus of *Micrathena* (Garrison et al., 2016). Additionally, to resolve relationships within three species of *Argiope*, we relied on an additional phylogeny (Scharff et al., 2019). This leaves two study species, *N. crucifera* and *N. oaxacensis*, to add to our phylogeny. *Neoscona arabesca* is the single representative of the genus in our original phylogeny. Lacking a phylogenetic study that resolves relationships among

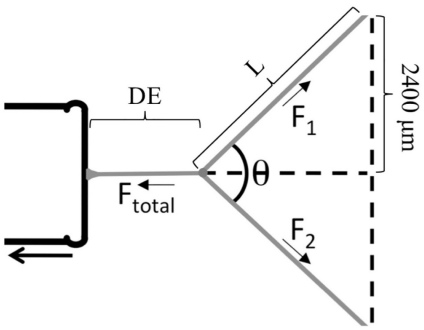

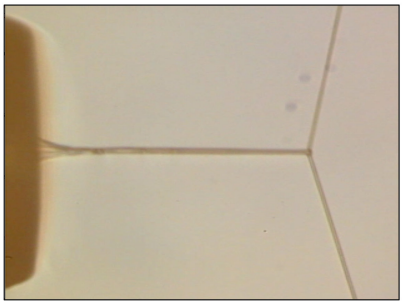

1. $L = 2400\ \mu m \div \sin(\theta/2)$
2. $AE = (L - 2400\ \mu m) \div 2400\ \mu m$
3. $F_1 = F_2 = YM \times \Sigma\ CSA_{AF} \times AE$
4. $F_{total} = 2 \times F_1 \times \sin(90° - (\theta/2))$
5. $CSA_{GF} = GV \div DE$
6. $Stress_T = F_{total} \div CSA_{GF}$
7. $Strain_T = Log_N((DE - DGC) \div DGC)$

AE = extension of axial line
YM = Young's modulus
CSA_{AF} = axial fiber cross sectional area
CSA_{GF} = glycoprotein filament cross sectional area
GV = glycoprotein volume
DGC = diameter of glycoprotein core when configured as a sphere

FIGURE 3 Diagram explaining how the elastic modulus of individual droplets are measured. Visualization to accompany the steps for measuring elastic modulus in the methods section. Modified from Figure 4 of Opell, Jain, et al., 2018, which from an open-source journal. Droplet extension image is from *Larinioides cornutus* at 55% RH

these species, *N. crucifera* was placed as sister to *N. arabesca* to the exclusion of *N. oaxacensis* (Figure 2). This placement was arbitrary, and the ensuing uncertainty that this placement may introduce to our PGLS results is addressed in the following paragraph. The branch lengths were then set to preserve the ultrametric character of the tree. Having a complete 16 species tree, we used PGLS to examine relationships among traits and plot phylomorphospace plots, carried out using the ape, caper, geiger and phytools packages in R (Orme et al., 2018; Paradis & Schliep, 2019; Pennell et al., 2014; R Core Team, 2019; Revell, 2012).

While the six taxa added to our input tree (Dimitrov et al., 2017) were necessary to utilize our material properties data, they may introduce uncertainty in our results. Four species: *A. pegnia*, *N. crucifera*, *N. oaxacensis* and *M. sagitatta* were added based on congeneric species already in our input tree (taxonomic information), rather than a phylogenetic analysis (Figure 2). While the placement of *A. aurantia* and *V. arenata* were based on other phylogenies, these were derived from different datasets that feature different sampling of spider diversity (Garrison et al., 2016; Scharff et al., 2019). What may compound this uncertainty is the varying nodal support across the branches of our input tree, with broad confidence intervals around the divergence times among these relationships as well. Therefore, it is necessary to examine alternate topologies and branch lengths to assess the influence of constructing our 16 species phylogeny in its present form (Figure 2). To assess the impact of adding species to our phylogeny, we created seven alternate phylogenies. Six of these alternate phylogenies featured a random placement of a single 'new' species (*A. pegnia*, *A. aurantia*, *N. crucifera*, *N. oaxacensis*, *M. sagitatta* or *V. arenata*). The seventh was a phylogeny where branch length was set to one across the entire 16 species topology. Using these trees, we implemented the sensiPhy R package to assess differences in the PGLS results (Paterno et al., 2018). We also used sensiPhy to determine if our sampling of taxa resulted in biased results in our spider mass and thread property analyses. In addition to the R packages mentioned, we also used SAS JMP for implementing thread characterization equations (SAS Institute Inc., Carey, NC).

3 | RESULTS

The values of each species' glycoprotein and flagelliform fibre material property are displayed together (Table 2). A PGLS analysis showed that, of these features, only glycoprotein and flagelliform elastic moduli were correlated, with glycoprotein elastic modulus being approximately one-sixth that of flagelliform fibres elastic modulus (Figure 4a, Table 3). The phylogenetic signal of glycoprotein and flagelliform fibre elastic moduli were 1.1 and 1.07, respectively. High elastic modulus values in one component are often associated

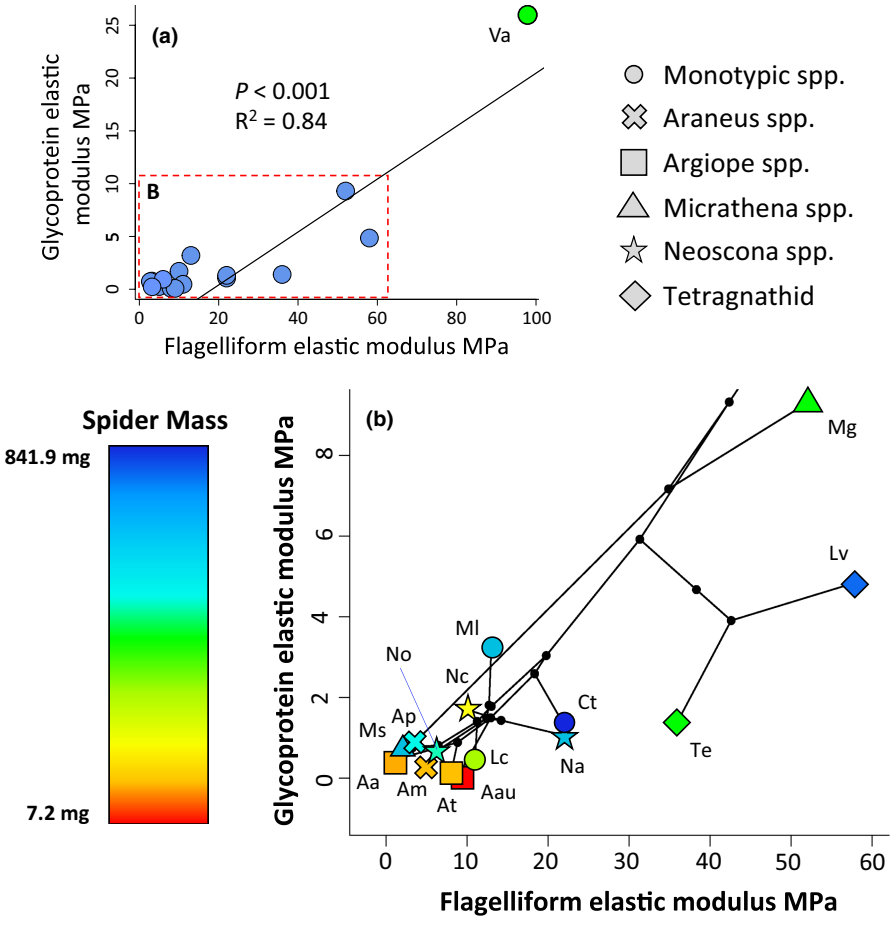

FIGURE 4 PGLS (a) and phylomorphospace (b) plots showing the relationship between the elastic modulus of each capture thread component. Increased elastic modulus of the flagelliform fibres is associated with increases in glycoprotein elastic modulus. The inset (4B) displays a close look and overlays mass and the identity of each species on a phylomorphospace plot. Abbreviations consist of the first letter of each species scientific name, except for *Argiope aurantia*, which uses Aau

TABLE 3 Each PGLS analysis and their results

Relationship	*p*	R^2
Glycoprotein elastic modulus versus flagelliform elastic modulus (MPa)	**<0.001**	0.85
Glycoprotein toughness versus flagelliform toughness (MJ/m^3)	0.35	0.06
Glycoprotein volume per mm of thread versus flagelliform volume per mm of thread	0.19	0.12
Spider mass (mg) vs.		
Glycoprotein elastic modulus (MPa)	0.59	0.02
Flagelliform elastic modulus (MPa)	0.45	0.04
Glycoprotein toughness (MJ/m^3)	0.56	0.02
Flagelliform toughness (MJ/m^3)	0.08	0.19
Glycoprotein volume per droplet (μm^3)	**0.01**	0.37
Flagelliform fibre cross-sectional area (μm^2)	**<0.001**	0.89
Droplets per millimetre	**0.007**	0.40

Note: Each PGLS regression is derived from a comparison of all 16 study species (Figure 2). *p* values in bold represent relationships that are plotted as figures (Figures 4 and 5, respectively). Bold values represent significant relationships, interpreted as such when $p < 0.05$.

with high values in the other component (Figures 4). Members of the family Tetragnathidae (*L. venusta* and *T. elongata*) had conspicuously lower glycoprotein elastic modulus values relative to flagelliform fibre values than did Araneidae species. In most cases congeneric species tended to cluster together, despite having different masses (Figure 4b). However, *M. gracilis* and *M. sagitatta* values were widely separated, with *M. gracilis* having much stiffer thread components. We found no correlation between the glycoprotein and flagelliform fibre toughness (Figure S1, Table 3). Toughness of flagelliform fibres displayed no phylogenetic signal, but glycoprotein toughness had a signal of 1. All other material properties listed in Table 2 (as well as spider mass and droplets per milometer in Table 1) had a signal of 0, with glycoprotein toughness being the only exception. There was no relationship between the amount of material invested per mm thread length of the two components (Table 3). Spider mass was not related to the elastic modulus or toughness of either thread components (Table 3). However, spider mass was positively correlated with glycoprotein volume per droplet and flagelliform fibre cross-sectional area and negatively correlated with droplets per millimetre thread length; that is, larger spiders tended to spin capture threads with larger, more widely spaced glue droplets (Table 3, Figure 5).

Using sensiPhy, we analysed our 16 species phylogeny with alternate topologies and branch lengths and their impact on our PGLS comparing glycoprotein and flagelliform fibre elastic modulus (Figure S1). These alternate trees had no impact on the significance of the PGLS, with all alternate topologies and branch lengths still significant under $p < 0.05$. Confidence intervals generated by this analysis can be visualized in Figure S1. Additionally, our sampling of orb weavers features a broad range of spider masses, but most of them fall under 100 mg, leaving species like *A. aurantia* as considerable outliers (Table 1). To detect if our sampling influences our three mass related PGLS analyses, we again employed sensiPhy, which was used to detect species biasing our results using the 'influ' family of codes (Paterno et al., 2018). *Argiope aurantia* was found to be influential when examining mass and its relationship with glycoprotein volume and flagelliform fibre cross-sectional area ($p < 0.001$ and 0.0001, respectively). This may be suspected as larger spiders are expected to spin larger threads glue droplets. However, when *A. aurantia* is removed form analyses, both relationships remain significant under $p < 0.05$. Interestingly, when searching for influential taxa in our mass and droplets per millimetre relationship, *C. turbinata* is found to be the most impactful species data. The smallest species included in this phylogeny has a dramatically higher droplets per millimetre than any other species, leading its significant impact on the data. However, a rerun PGLS still returns a significant *p* value of 0.01.

4 | DISCUSSION

4.1 | Synergy between capture thread material properties

Glycoprotein and flagelliform fibres interact to retain insects that strike the web. The adhesive performance of the thread is conditioned by its elasticity, with modelling and empirical work revealing a balance of silk elasticity and stickiness that is crucial to adhesion (Guo et al., 2018; Opell, Clouse, & Andrews, 2018). Therefore, it is significant that, of the hypothesized associations between adhesive protein and flagelliform fibres, the only correlated material property was elastic modulus (Figures 4 and 5, Table 3). Maintaining this balance appears to ensure that the structural integrity of the bridge is maintained during adhesion (Guo et al., 2018). The support line of a loaded capture thread assumes a parabolic shape. Therefore, a disproportionate increase in glycoprotein elastic modulus would cause the outer droplets to pull-off before inner droplet extension was initiated, due to the support line's parabola having a shallow focus. A disproportionate decrease in glycoprotein elastic modulus would have the same effect, but due to a parabola with a deep focus. An unbalanced stiffening of the flagelliform fibres would also reduce the ability of both thread components to contribute to the work done in pulling a thread from a surface. This work has been shown to make an equally large contribution to insect retention time (Opell et al., 2019; Sahni et al., 2010). Thus, the strong linkage of these elastic moduli has been maintained by selection to optimize capture thread performance.

Consistent with their roles in capture thread function, we documented that the toughness of capture thread glycoprotein is less than that of the thread's flagelliform fibres (Table 2). However, our analysis did not support a clear linkage of the toughness of these components (Table 3). Several technical considerations may have prevented us from documenting this linkage. As noted, in our analyses glycoprotein toughness was limited by a droplet's adhesive failure rather than protein rupture. This is consistent with the observation that the glue droplets release before enough force is accumulated to break a thread's flagelliform fibres (Agnarsson

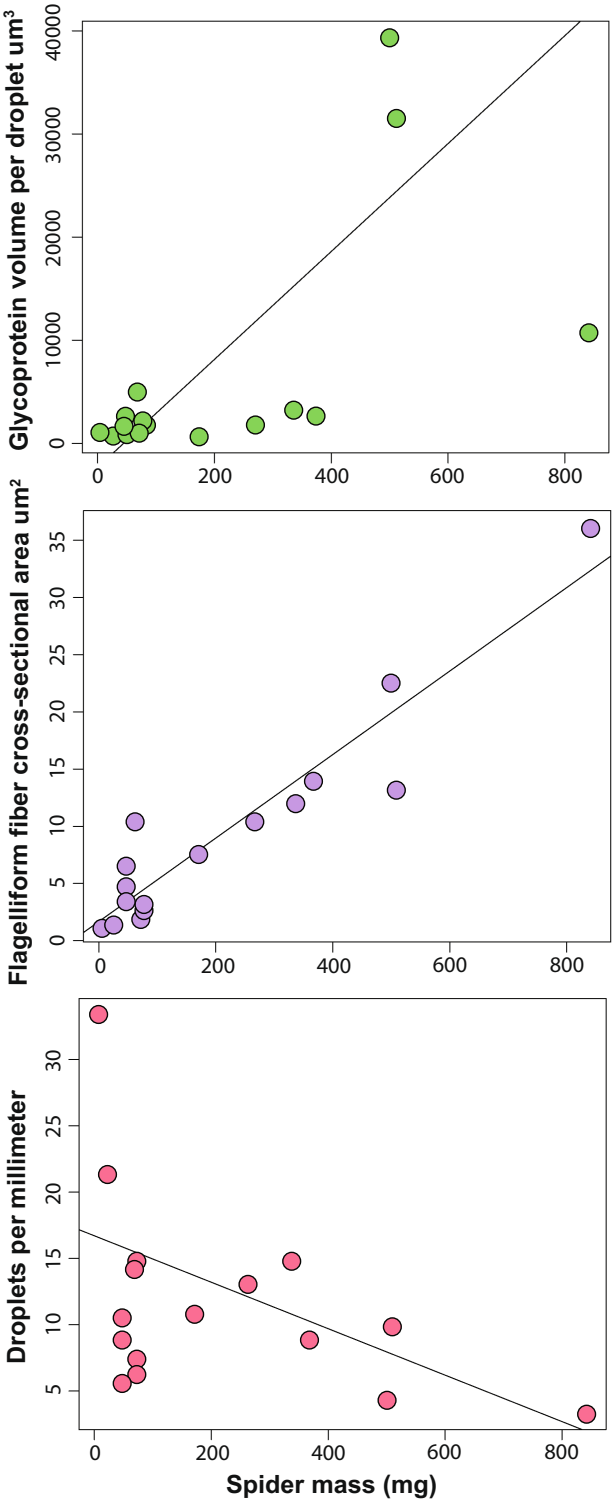

FIGURE 5 PGLS plots of spider mass against capture thread features. Of our PGLS analyses, these are the only three to produce significant ($p < 0.05$) relationships. Higher spider mass is associated with increased glycoprotein volume and flagelliform cross-sectional area (first two graphs). Larger spiders appear to build capture threads with larger and further spaced droplets (first and third plots)

& Blackledge, 2009). However, when the toughness of flagelliform fibres is characterized in the laboratory, threads are extended until they break. Thus, during normal capture thread performance only a portion of flagelliform fibre actual toughness is realized. If this realized flagelliform fibre toughness were known it might be correlated with expressed glycoprotein toughness. While the phylogeny that underlies these results has been altered to match our material property data set, our PGLS results remain robust to alternate topologies and branch lengths (Figure S1).

4.2 | Material investment in capture thread components

Orb-web weavers differ greatly in mass, over a hundredfold in the case of species included in this study, but spider size and its impact on adhesive performance is not fully understood. Greater spider mass has been linked with higher insect stopping potential, but the effect of mass on the material properties of the capture thread is not explicitly known (Sensenig et al., 2010). Our comparative phylogenetic analyses found no evidence that spider mass is correlated to the toughness or elastic modulus of capture thread glycoprotein or flagelliform fibres (Table 3). This may be because the performance of a thread's components is determined by a combination of their material properties and the amount of material invested in each component.

Flagelliform fibre cross-sectional area and spider mass are positively correlated, a relationship explained by the tendency for larger spiders to spin thicker flagelliform fibres (Figure 5). Glycoprotein volume exhibits the same pattern. Smaller spiders also have a greater number of smaller droplets per millimetre thread length, as shown by a positive correlation of glycoprotein volume with spider mass (Figure 5). It should be noted that species on the upper (*A. aurantia*) and lower (*C. turbinata*) limits of spider mass may influence our results, but their removal does not dissolve their respective relationships displayed in Figure 5. However, flagelliform fibre cross-sectional area and glycoprotein volume are not correlated and remain unrelated when scaled to flagelliform fibre and glycoprotein volume per millimetre thread length (Table 3). Differences in spiral spacing may be confounding this relationship, as more widely spaced capture spirals experience greater individual stress upon prey impact than closely spaced spirals. The ability of natural selection to strengthen a flagelliform fibre appears to be constrained by two factors: 1. The direct relationship of flagelliform fibre elastic modulus to adhesive protein elastic modulus and 2. The inherent relationship of flagelliform fibre elastic modulus and flagelliform fibre toughness. Therefore, this leaves flagelliform fibre diameter as the principal feature upon which selection can act to strengthen a capture thread.

5 | CONCLUSION

Spider orb webs exhibit many levels of integration, which correspond to the material properties and roles of their threads. During a short time span, prey capture progresses from insect interception, during which a web's radial threads are largely responsible for absorbing the force of prey impact, to prey retention when capture thread's glue droplets contact an insect and stretch to transfer force to flagelliform fibres. The material

properties of these web elements are structured according to their roles, with radial threads, flagelliform fibres and adhesive proteins exhibiting decreasing stiffness (Opell, Clouse, & Andrews, 2018). We demonstrate that natural selection on flagelliform fibre and glycoprotein elastic modulus has been shaped by the interdependence of these capture thread components. This linkage appears to constrain how selection acts because a disproportionate change in one component's property would reduce the functionality of the adhesive (Guo et al., 2018). Thus, to preserve the synergistic pattern, natural selection must simultaneously maintain the distinct contribution of each component. We show that this occurs when glycoprotein elastic modulus is typically one-sixth that of flagelliform fibre elastic modulus (Figure 4). If future studies can measure the 'expressed toughness' of the flagelliform fibre during thread adhesion, this synergy may also extend to this property. Ultimately, successful adhesion of the capture during a prey depends on the precise functional integration of many thread components, both chemical and biomechanical.

AUTHOR CONTRIBUTIONS

SDK and BDO conceptualized the study, collectedand tested capture threads of four species whose properties were added to those that were previously published, and composed the first manuscript draft. SC-G characterized these four species' flagelliform fibre material properties and helped improve the manuscript.

BDO provided funding through NSF for this study on grant: IOS-1755028.

ACKNOWLEDGEMENTS

We would like to acknowledge Dimitar Dimitrov for providing the base phylogeny for this work. SDK would like to acknowledge Marth Muñoz and Josef Uyeda for their feedback on the phylogenetic aspects of this study. We thank Nadia Ayoub for providing access to *M. sagitatta* webs and spiders. Tierney C. Bougie collected *Argiope argentata* specimens and Sarah Morris and Luca DuMez helped characterize this species' glue droplets.

CONFLICT OF INTEREST

The authors have no conflict of interest to declare.

DATA AVAILABILITY STATEMENT

The data that support the findings of this study and code used to provide results are openly available in Dryad: https://doi.org/10.6086/D1M97D

PEER REVIEW

The peer review history for this article is available at https://publons.com/publon/10.1111/jeb.14025.

ORCID

Sean D. Kelly https://orcid.org/0000-0001-6815-8558
Brent D. Opell https://orcid.org/0000-0002-1830-0752
Sandra M. Correa-Garwhal https://orcid.org/0000-0002-6889-2688

REFERENCES

Agnarsson, I., & Blackledge, T. A. (2009). Can a spider web be too sticky? Tensile mechanics constrains the evolution of capture spiral stickiness in orb-weaving spiders. *Journal of Zoology*, *278*, 134–140.

Amarpuri, G., Chaurasia, V., Jain, D., Blackledge, T. A., & Dhinojwala, A. (2015). Ubiquitous distribution of salts and proteins in spider glue enhances spider silk adhesion. *Scientific Reports*, *5*, 9030.

Amarpuri, G., Zhang, C., Blackledge, T. A., & Dhinojwala, A. (2017). Adhesion modulation using glue droplet spreading in spider capture silk. *Journal of the Royal Society Interface*, *14*, 20170228.

Amarpuri, G., Zhang, C., Diaz, C., Opell, B. D., Blackledge, T. A., & Dhinojwala, A. (2015). Spiders tune glue viscosity to maximize adhesion. *American Chemical Society*, *9*, 11472–11478.

Blackledge, T. A., & Gillespie, R. G. (2002). Estimation of capture areas in spider orb webs in relation to asymmetry. *Journal of Arachnology*, *30*, 70–77.

Blackledge, T. A., & Hayashi, C. Y. (2006). Silken toolkits: Biomechanics of silk fibers spun by the orb web spider Argiope argentata (Fabricius 1775). *The Journal of Experimental Biology*, *209*, 2452–2461.

Blackledge, T. A., Kuntner, M., & Agnarsson, I. (2011). The form and function of spider orb webs: Evolution from silk to ecosystems. *Advances in Insect Physiology*, *41*, 175–262.

Bradley, R. A. (2013). *Common spiders of North America*. University of Califronia Press.

Chacón, P., & Eberhard, W. G. (1980). Factors affecting numbers and kinds of prey caught in artificial spider webs, with considerations of how orb webs trap prey. *Bulletin of the British Arachnological Society*, *5*, 29–38.

Coddington, J. A. (1989). Spinneret silk spigot morphology: Evidence for the monophyly of Orbweaving spiders, Cyrtophorinae (Araneidae), and group Theridiidae plus Nesticidae. *Journal of Arachnology*, *17*, 71–95.

Dickinson, G. H., Vega, I. E., Wahl, K. J., Orihuela, B., Beyley, V., Rodriguez, E. N., Everett, R. K., Bonaventura, J., & Rittschof, D. (2009). Barnacle cement: A polymerization model based on evolutionary concepts. *The Journal of Experimental Biology*, *212*, 3499–3510.

Dimitrov, D., Benavides, L. R., Arnedo, M. A., Giribet, G., Griswold, C. E., Scharff, N., & Hormiga, G. (2017). Rounding up the usual suspects: A standard target-gene approachfor resolving the interfamilial phylogenetic relationships ofecribellate orb-weaving spiders with a new family-rank classification(Araneae, Araneoidea). *Cladistics*, *33*, 221–250.

Edmonds, D. T., & Vollrath, F. (1992). The contribution of atmospheric water vapour to the formation and efficiency of a Spider's capture web. *Proceeding of the Royal Society B: Biological Sciences*, *248*, 145–148.

Felsenstein, J. (1985). Phylogenies and the comparative method. *The American Naturalist*, *125*, 1–15.

Garamszegi, L. Z. (2014). *Modern phylogenetic comparative methods and their application in evolutionary biology*. Springer.

Garrison, N. L., Rodriguez, J., Agnarsson, I., Coddington, J. A., Griswold, C. E., Hamilton, C. A., Hedin, M., Kocot, K. M., Ledford, J. M., & Bond, J. E. (2016). Spider phylogenomics: Untangling the spider tree of life. *PeerJ*, *4*, 1719–1754.

Greenstone, M. H., & Bennett, A. F. (1980). Foraging strategy and metabolic rate in spiders. *Ecology*, *61*, 1255–1259.

Guo, Y., Chang, Z., Guo, H. Y., Fang, W., Li, Q., Zhao, H. P., Feng, X. Q., & Gao, H. (2018). Synergistic adhesion mechanisms of spider capture silk. *Journal of the Royal Society Interface*, *15*, 20170894.

Guo, Y., Zhao, H.-P., Feng, X.-Q., & Gao, H. (2019). On the robustness of spider capture silk's adhesion. *Extreme Mechanics Letters*, *29*, 100477.

Huang, Y., Wang, Y., Sun, L., Agrawal, R., & Zhang, M. (2015). Sundew adhesive: A naturally occurring hydrogel. *Journal of the Royal Society Interface*, *12*, 20150226.

Jain, D., Amarpuri, G., Fitch, J., Blackledge, T. A., & Dhinojwala, A. (2018). Role of hygroscopic low molecular mass compounds in humidity responsive adhesion of Spider's capture silk. *Biomacromolecules*, *19*, 3048–3057.

Kelly, S. D., Opell, B. D., & Owens, L. L. (2019). Orb weaver glycoprotein is a smart biological material, capable of repeated adhesion cycles. *The Science of Nature*, *106*, 3–4.

Krausko, M., Perutka, Z., Šebela, M., Šamajová, O., Šamaj, J., Novák, O., & Pavlovič, A. (2017). The role of electrical and jasmonate signalling in the recognition of captured prey in the carnivorous sundew plant Drosera capensis. *The New Phytologist*, *213*, 1818–1835.

Liao, C.-P., Blamires, S. J., Hendricks, M. L., & Opell, B. D. (2015). A re-evaluation of the formula to estimate the volume of orb web glue droplets. *Journal of Arachnology*, *43*, 97–100.

Mead-Hunter, R., King, A. J. C., & Mullins, B. J. (2012). Plateau Rayleigh instability simulation. *Langmuir*, *28*, 6731–6735.

Olivencia, A. O., Claver, J. P. C., & Alcatraz, J. A. D. (1995). Floral and reproductive biology of Drosophyllum lusitanicum (L.) link (Droseraceae). *Botanical Journal of the Linnean Society*, *118*, 331–351.

Opell, B. D., Burba, C. M., Deva, P. D., Kin, M. H. Y., Rivas, M. X., Elmore, H. M., & Hendricks, M. L. (2019). Linking properties of an orb-weaving spider's capture thread glycoprotein adhesive and flagelliform fiber components to prey retention time. *Ecology and Evolution*, *9*, 1–14.

Opell, B. D., Clouse, M. E., & Andrews, S. F. (2018). Elastic modulus and toughness of orb spider glycoprotein glue. *PLoS One*, *13*, e0196972.

Opell, B. D., Elmore, H. M., & Hendricks, M. L. (2021). Humidity mediated performance and material properties of orb weaving spider adhesive droplets. *Acta Biomaterialia*, *131*, 440–451.

Opell, B. D., & Hendricks, M. L. (2009). The adhesive delivery system of viscous capture threads spun by orb-weaving spiders. *The Journal of Experimental Biology*, *212*, 3026–3034.

Opell, B. D., & Hendricks, M. L. (2010). The role of granules within viscous capture threads of orb-weaving spiders. *The Journal of Experimental Biology*, *213*, 339–346.

Opell, B.D., Jain, D., Dhinojwala, A. & Blackledge, T.A. 2018. Tuning orb spider glycoprotein glue performance to habitat humidity. *The Journal of Experimental Biology*, *221*, Tuning orb spider glycoprotein glue performance to habitat humidity.

Opell, B. D., Markley, B. J., Hannum, C. D., & Hendricks, M. L. (2008). The contribution of axial fiber extensibility to the adhesion of viscous capture threads spun by orb-weaving spiders. *The Journal of Experimental Biology*, *211*, 2243–2251.

Opell, B. D., Sigler, M. A., & Karinshak, S. E. (2011). Humidity affects the extensibility of an orb-weaving spider's viscous thread droplets. *The Journal of Experimental Biology*, *214*, 2988–2993.

Opell, B. D., & Stellwagen, S. D. (2019). Properties of orb weaving spider glycoprotein glue change during Argiope trifasciata web construction. *Scientific Reports*, *9*, 1–11.

Orme, D., Freckleton, R., Thomas, G., Petzoldt, T., Fritz, S.A., Isaac, N., Pearse W. 2018. *Caper: Comparative analyses of phylogenetics and evolution in R*.

Pagel, M. (1999). Inferring historical patterns of biological evolution. *Nature*, *401*, 877–884.

Paradis, E., & Schliep, K. (2019). Ape 5.0: An environment for modern phylogenetics and evolutionary analyses in R. *Bioinformatics*, *35*, 526–528.

Paterno, G. B., Penone, C., & Werner, G. D. A. (2018). sensiPhy: An r-package for sensitivity analysis in phylogenetic comparative methods. *Methods in Ecology and Evolution*, *9*, 1461–1467.

Pennell, M. W., Eastman, J. M., Slater, G. J., Brown, J. W., Uyeda, J. C., Fitzjohn, R. G., et al. (2014). Geiger v2.0: An expanded suite of methods for fitting macroevolutionary models to phylogenetic trees. *Bioinformatics*, *30*, 2216–2218.

R Core Team. (2019). *R: A language and environment for statistical computing*. R Foundation for Statistical Computing.

Revell, L. J. (2012). Phytools: An R package for phylogenetic comparative biology (and other things). *Methods in Ecology and Evolution*, *3*, 217–223.

Sahni, V., Blackledge, T. A., & Dhinojwala, A. (2010). Viscoelastic solids explain spider web stickiness. *Nature Communications*, *1*, 1–4.

Sahni, V., Blackledge, T. A., & Dhinojwala, A. (2011). Changes in the adhesive properties of spider aggregate glue during the evolution of cobwebs. *Scientific Reports*, *1*, 1–8.

Sahni, V., Miyoshi, T., Chen, K., Jain, D., Blamires, S. J., Blackledge, T. A., & Dhinojwala, A. (2014). Direct solvation of glycoproteins by salts in spider silk glues enhances adhesion and helps to explain the evolution of modern spider orb webs. *Biomacromolecules*, *15*, 1225–1232.

Santos, R., da Costa, G., Franco, C., Gomes-Alves, P., Flammang, P., & Coelho, A. V. (2009). First insights into the biochemistry of tube foot adhesive from the sea urchin Paracentrotus lividus (Echinoidea, Echinodermata). *Marine Biotechnology*, *11*, 686–698.

Scharff, N., Coddington, J. A., Blackledge, T. A., Agnarsson, I., Framenaue, V. W., Szuts, T., et al. (2019). Phylogeny of the orb-weaving spider family Araneidae (Araneae: Araneoidea). *Cladistics*, *36*, 1–21.

Sensenig, A. T., Agnarsson, I., & Blackledge, T. A. (2010). Behavioral and biomaterial coevolution in spider orb webs. *Journal of Evolutionary Biology*, *23*, 1839–1856.

Sensenig, A. T., Lorentz, K. A., Kelly, S. P., & Blackledge, T. A. (2012). Spider orb webs rely on radial threads to absorb prey kinetic energy. *Journal of the Royal Society Interface*, *9*, 1880–1891.

Singla, S., Amarpuri, G., Dhopatkar, N., Blackledge, T. A., & Dhinojwala, A. (2018). Hygroscopic compounds in spider aggregate glue remove interfacial water to maintain adhesion in humid conditions. *Nature Communication*, *9*, 1890.

Stark, A. Y., Davis, H. R., & Harrison, W. K. (2019). Shear adhesive performance of leaf-cutting ant workers (Atta cephalotes). *Biotropica*, *51*, 572–580.

Swanson, B. O., Blackledge, T. A., Summers, A. P., & Hayashi, C. Y. (2006). Spider dragline silk: Correlated and mosaic evolution in high-performance biological materials. *Evolution*, *8*, 2539–2551.

Tillinghast, E. K., Townley, M. A., Wight, T. N., Uhlenbruck, G., & Janssen, E. (1993). The adhesive glycoprotein of the orb of Argiope aurantia (Araneae, Araneidae). *Materials Research Society Symposium Proceedings*, *259*, 154–165.

Townley, M. A., Bernstein, D. T., Gallagher, K. S., & Tillinghast, E. K. (1991). Comparative study of orb web hygroscopicity and adhesive spiral composition in three araneid spiders. *The Journal of Experimental Zoology*, *259*, 154–165.

Townley, M. A., & Tillinghast, E. K. (2013). Aggregate silk gland secretions of Araneoid spiders. In W. Nentwig (Ed.), *Aggregate silk gland secretions of Araneoid spiders*. Springer-Verlag.

Uetz, G. W., Johnson, A. D., & Schemske, D. W. (1978). Web placement, web structure, and prey capture in orb-weaving spiders. *Bulletin of the British Arachnological Society*, *4*, 141–148.

Vollrath, F., & Tillinghast, E. K. (1991). Glycoprotein glue beneath a spider web's aqueous coat. *Naturwissenschaften*, *78*, 557–559.

Waite, H. J. (2017). Mussel adhesion - essential footwork. *The Journal of Experimental Biology*, *220*, 517–530.

SUPPORTING INFORMATION

Additional supporting information may be found in the online version of the article at the publisher's website.

How to cite this article: Kelly, S. D., Opell, B. D., & Correa-Garwhal, S. M. (2022). Correlated evolution between orb weaver glue droplets and supporting fibres maintains their distinct biomechanical roles in adhesion. *Journal of Evolutionary Biology*, *35*, 879–890. https://doi.org/10.1111/jeb.14025